



**HAL**  
open science

## Intercomparison study of atmospheric $^{222}\text{Rn}$ and $^{222}\text{Rn}$ progeny monitors

Claudia Grossi, Scott Chambers, Olivier Llido, Felix Vogel, Victor Kazan, Alessandro Capuana, Sylvester Werczynski, Roger Curcoll, Marc Delmotte, Arturo Vargas, et al.

### ► To cite this version:

Claudia Grossi, Scott Chambers, Olivier Llido, Felix Vogel, Victor Kazan, et al.. Intercomparison study of atmospheric  $^{222}\text{Rn}$  and  $^{222}\text{Rn}$  progeny monitors. Atmospheric Measurement Techniques, 2020, 13 (5), pp.2241-2255. 10.5194/amt-13-2241-2020 . hal-02615025

HAL Id: hal-02615025

<https://hal.science/hal-02615025v1>

Submitted on 2 Jun 2020

**HAL** is a multi-disciplinary open access archive for the deposit and dissemination of scientific research documents, whether they are published or not. The documents may come from teaching and research institutions in France or abroad, or from public or private research centers.

L'archive ouverte pluridisciplinaire **HAL**, est destinée au dépôt et à la diffusion de documents scientifiques de niveau recherche, publiés ou non, émanant des établissements d'enseignement et de recherche français ou étrangers, des laboratoires publics ou privés.



Distributed under a Creative Commons Attribution 4.0 International License



## Intercomparison study of atmospheric $^{222}\text{Rn}$ and $^{222}\text{Rn}$ progeny monitors

Claudia Grossi<sup>1,2</sup>, Scott D. Chambers<sup>3</sup>, Olivier Llido<sup>4</sup>, Felix R. Vogel<sup>5</sup>, Victor Kazan<sup>4</sup>, Alessandro Capuana<sup>6</sup>, Sylvester Werczynski<sup>3</sup>, Roger Curcoll<sup>7,8</sup>, Marc Delmotte<sup>4</sup>, Arturo Vargas<sup>1</sup>, Josep-Anton Morguí<sup>7,9</sup>, Ingeborg Levin<sup>6</sup>, and Michel Ramonet<sup>4</sup>

<sup>1</sup>Institut de Tècniques Energètiques (INTE), Universitat Politècnica de Catalunya (UPC), Barcelona, Spain

<sup>2</sup>Physics Department, Universitat Politècnica de Catalunya (UPC), Barcelona, Spain

<sup>3</sup>Environmental Research, ANSTO, Lucas Heights, Australia

<sup>4</sup>Laboratoire des Sciences du Climat et de l'Environnement, Université Paris-Saclay (LSCE/IPSL, CEA-CNRS-UVSQ), Gif-sur-Yvette, France

<sup>5</sup>Climate Research Division, Environment and Climate Change Canada, Toronto, Canada

<sup>6</sup>Institut für Umweltp Physik (IUP), Heidelberg University, Heidelberg, Germany

<sup>7</sup>Institut de Ciència i Tecnologia Ambientals (ICTA), Universitat Autònoma de Barcelona (UAB), Cerdanyola del Vallès, Spain

<sup>8</sup>Chemical Department, Universitat Politècnica de Catalunya (UPC), Barcelona, Spain

<sup>9</sup>Departament Biologia Evolutiva, Ecologia i Ciències Ambientals, Universitat de Barcelona (UB), Barcelona, Spain

**Correspondence:** Claudia Grossi (claudia.grossi@upc.edu)

Received: 7 October 2019 – Discussion started: 6 November 2019

Revised: 6 March 2020 – Accepted: 26 March 2020 – Published: 8 May 2020

**Abstract.** The use of the noble gas radon ( $^{222}\text{Rn}$ ) as a tracer for different research studies, for example observation-based estimation of greenhouse gas (GHG) fluxes, has led to the need of high-quality  $^{222}\text{Rn}$  activity concentration observations with high spatial and temporal resolution. So far a robust metrology chain for these measurements is not yet available.

A portable direct atmospheric radon monitor (ARMON), based on electrostatic collection of  $^{218}\text{Po}$ , is now running at Spanish stations. This monitor has not yet been compared with other  $^{222}\text{Rn}$  and  $^{222}\text{Rn}$  progeny monitors commonly used at atmospheric stations.

A 3-month intercomparison campaign of atmospheric  $^{222}\text{Rn}$  and  $^{222}\text{Rn}$  progeny monitors based on different measurement techniques was realized during the fall and winter of 2016–2017 to evaluate (i) calibration and correction factors between monitors necessary to harmonize the atmospheric radon observations and (ii) the dependence of each monitor's response in relation to the sampling height and meteorological and atmospheric aerosol conditions.

Results of this study have shown the following. (i) All monitors were able to reproduce the atmospheric radon variability on a daily basis. (ii) Linear regression fits between the monitors exhibited slopes, representing the correction factors, between 0.62 and 1.17 and offsets ranging between  $-0.85$  and  $-0.23\text{ Bq m}^{-3}$  when sampling 2 m above ground level (a.g.l.). Corresponding results at 100 m a.g.l. exhibited slopes of 0.94 and 1.03 with offsets of  $-0.13$  and  $0.01\text{ Bq m}^{-3}$ , respectively. (iii) No influence of atmospheric temperature and relative humidity on monitor responses was observed for unsaturated conditions at 100 m a.g.l., whereas slight influences (order of  $10^{-2}$ ) of ambient temperature were observed at 2 m a.g.l. (iv) Changes in the ratio between  $^{222}\text{Rn}$  progeny and  $^{222}\text{Rn}$  monitor responses were observed under very low atmospheric aerosol concentrations.

Results also show that the new ARMON could be useful at atmospheric radon monitoring stations with space restrictions or as a mobile reference instrument to calibrate in situ  $^{222}\text{Rn}$  progeny monitors and fixed radon monitors. In the near future a long-term comparison study between ARMON,

HRM, and ANSTO monitors would be useful to better evaluate (i) the uncertainties of radon measurements in the range of a few hundred millibecquerels per cubic meter to a few becquerels per cubic meter and (ii) the response time correction of the ANSTO monitor for representing fast changes in the ambient radon concentrations.

## 1 Introduction

Over continents, the natural radioactive noble gas radon ( $^{222}\text{Rn}$ ) (half-life  $T_{1/2} = 3.8$  d) is continuously generated within the soil from the decay of radium ( $^{226}\text{Ra}$ ) (Nazaroff and Nero, 1988), and it can then escape into the atmosphere by diffusion, depending on soil characteristics and meteorological conditions (Grossi et al., 2011; López-Coto et al., 2013; Karstens et al., 2015). The global  $^{222}\text{Rn}$  source into the atmosphere is mainly restricted to land surfaces (Szegvary et al., 2009; Karstens et al., 2015), with the  $^{222}\text{Rn}$  flux from water surfaces considered negligible for most applications (Schery and Huang, 2004).

In recent decades the atmospheric scientific community has been addressing different research topics using  $^{222}\text{Rn}$  as a tracer. Examples of such applications include the improvement of inverse transport models (Hirao et al., 2010), the improvement of chemical transport models (Jacob and Prather, 1990; Chambers et al., 2019a), the study of atmospheric transport and mixing processes within the planetary boundary layer (Zahorowski et al., 2004; Galmarini, 2006; Baskaran, 2011; Chambers et al., 2011, 2016, 2019b; Williams et al., 2011, 2013; Vogel et al., 2013; Vargas et al., 2015; Baskaran, 2016), the experimental estimation of greenhouse gas (GHG) fluxes (Levin et al., 1999, 2011; Vogel et al., 2012; Wada et al., 2013; Grossi et al., 2018), and others listed in Grossi et al. (2016).

In light of this, atmospheric  $^{222}\text{Rn}$  measurements are being carried out at numerous monitoring stations of GHG concentrations and air quality using three fundamentally different measurement principles: one filter, two filters, and electrostatic deposition (Stockburger and Sittkus, 1966; Hopke, 1989; Whittlestone and Zahorowski, 1998; Paatero et al., 1998; Levin et al., 2002). The two most commonly employed measurement systems at European  $^{222}\text{Rn}$  monitoring stations are the dual-flow-loop two-filter monitor (Whittlestone and Zahorowski, 1998; Zahorowski et al., 2004; Chambers et al., 2011, 2014, 2018; Griffiths et al., 2016), which samples and measures radon directly, and the one-filter monitors, of which several kinds are in use (e.g., Stockburger and Sittkus, 1966; Polian, 1986; Paatero et al., 1998; Levin et al., 2002), which sample and measure aerosol-bound radon progeny. Finally, a third method is being used at several Spanish atmospheric stations (Vargas et al., 2015; Hernández-Ceballos et al., 2015; Grossi et al., 2016, 2018; Frank et al., 2016; Gutiérrez-Álvarez et al., 2019). This type

of instrument performs a direct measurement of  $^{222}\text{Rn}$  and  $^{220}\text{Rn}$  (thoron) activity concentrations using the already existing method based on the electrostatic deposition of  $^{218}\text{Po}$  and  $^{216}\text{Po}$ , respectively (Hopke, 1989; Tositti et al., 2002; Grossi et al., 2012).

The diversity of these three aforementioned measurement techniques could introduce biases or compatibility issues that would limit the comparability of the results obtained by independent studies and the subsequent application of atmospheric radon data for regional to global investigations (e.g., Schmithüsen et al., 2017). Thus, a comparative assessment of all the experimental techniques applied for atmospheric  $^{222}\text{Rn}$  activity concentration measurements and a harmonization of their datasets are needed, as suggested by the International Atomic Energy Agency (IAEA, 2012).

Xia et al. (2010) carried out a comparison of the response of a dual-flow-loop two-filter detector from the Australian Nuclear Science and Technology Organisation (ANSTO, Whittlestone and Zahorowski 1998) and a one-filter monitor ( $\alpha/\beta$  Monitor P3) manufactured by the Bundesamt für Strahlenschutz, Germany (BfS) (Stockburger and Sittkus, 1966), for atmospheric  $^{222}\text{Rn}$  measurements under various meteorological conditions at 2.5 m above ground level (a.g.l.) over 1 year. Their results showed that both systems followed the same patterns and produced very similar results most of the time, except under specific meteorological conditions such as when precipitation or the proximity of the forest canopy could remove short-lived progeny from the air mass to be measured by the one-filter monitor. However, Xia et al. (2010) did not find a clear relationship between precipitation intensity and the ratio between progeny-derived  $^{222}\text{Rn}$  and  $^{222}\text{Rn}$  activity concentration to convert the progeny signal to  $^{222}\text{Rn}$  activity concentration.

Grossi et al. (2016) presented results from two short (about 7–9 d) comparisons between a one-filter monitor from Heidelberg University (Heidelberg Radon Monitor, HRM; Levin et al., 2002) and an atmospheric radon monitor (ARMON; Grossi et al., 2012), an electrostatic deposition monitor from the Universitat Politècnica de Catalunya (UPC). The two comparison campaigns were carried out at a coastal and a mountain site, with sampling in both cases from 10 m a.g.l. These comparisons revealed that the responses of both monitors were in agreement except for water-saturated atmospheric conditions or periods of rainfall. Again, the quantity of comparison data was not sufficient to confirm any statistical correlation.

Loss of aerosols in the air intake systems can also complicate the derivation of  $^{222}\text{Rn}$  activity concentrations from one-filter systems such as the HRM. Levin et al. (2017) carried out an assessment of  $^{222}\text{Rn}$  progeny loss in long tubing by laboratory and field experiments. Results of these experiments, for 8.2 mm inner diameter (i.d.) Decabon tubing, gave an empirical correction function for  $^{222}\text{Rn}$  progeny measurements, which enables the correction of measurements for this

specific experimental setup (e.g., tubing type and diameter, flow rate, aerosol size distribution).

Finally, Schmithüsen et al. (2017) conducted an extensive European-wide  $^{222}\text{Rn}/^{222}\text{Rn}$  progeny comparison study in order to evaluate the comparative performance of one-filter and two-filter measurement systems, determining potential systematic biases between them and estimating correction factors that could be applied to harmonize  $^{222}\text{Rn}$  activity concentration estimates for their use as a tracer in various atmospheric applications. In this case, the authors employed a HRM monitor as the reference device. It was taken to nine European measurement stations to run for at least 1 month at each of them. This monitor was run in parallel to other one-filter and two-filter radon monitors operating at each station of interest.

Although several intercomparison campaigns have been carried out in the past, none of them have included simultaneous observations from one-filter, two-filter, and electrostatic deposition methods. Here, we present the results of a 3-month intercomparison campaign carried out in the fall and winter of 2016–2017 in Gif-sur-Yvette (France) where, for the first time, co-located measurements from monitors based on the three measurement principles were included. Two two-filter  $^{222}\text{Rn}$  monitors, two single-filter  $^{222}\text{Rn}$  progeny monitors, and an electrodeposition monitor were run simultaneously under different meteorological and aerosol conditions sampling from heights of 2 and 100 m a.g.l.

The main objectives of the present study were to (i) compare the calibration and correction factors between all monitors required to derive harmonized atmospheric radon activity concentrations and (ii) analyze the influence that meteorological and environmental parameters, as well as sampling height, can have on the final determined  $^{222}\text{Rn}$  activity concentration.

In the present paper the applied methodology is reported, including a short presentation of the  $^{222}\text{Rn}/^{222}\text{Rn}$  progeny monitors participating in the campaigns, the sampling sites, and the statistical analysis carried out. Finally, the outcomes of the present study are discussed and compared with the ones from Schmithüsen et al. (2017).

## 2 Methods

In Sect. 2.1 a short description is given of the monitors compared in the experiment, mainly focusing on measurement techniques, instrument calibration, and maintenance. The main characteristics of these monitors are then summarized in Table 1. Section 2.2 presents the French atmospheric stations of Orme de Mérisiers (ODM) and Saclay (SAC) where the two phases of the intercomparison campaign were realized. Section 2.3 briefly describes the devices used to measure the environmental parameters and the atmospheric aerosol concentration at the above sites during the experi-

ments. Finally, the statistical analysis applied is described in Sect. 2.4.

### 2.1 $^{222}\text{Rn}$ and $^{222}\text{Rn}$ progeny monitors

#### 2.1.1 Direct methods

##### Dual-flow-loop two-filter detectors

The two 1500 L dual-flow-loop two-filter detectors included in this exercise were designed and built at the Australian Nuclear Science and Technology Organisation (ANSTO). This model of detector, which will henceforth be named ANSTO, is based on a previous design by Thomas and Leclare (1970), with some early iterations of the modified design being described by Whittlestone and Zahorowski (1998) and Brunke et al. (2002). The subsequent evolution of two-filter detectors in recent decades, and the current principle of operation, has been described in detail by Williams and Chambers (2016) and Griffiths et al. (2016).

During the measurement campaign ambient air was sampled continuously at a rate of about  $83\text{ L min}^{-1}$  through a 50 mm i.d. HDPE inlet tube and a 400 L delay volume to allow decay of the short-lived  $^{220}\text{Rn}$  ( $T_{1/2} = 56\text{ s}$ ). The air stream then passes through the first filter, which removes all ambient aerosols as well as  $^{222}\text{Rn}$  and  $^{220}\text{Rn}$  progeny. The filtered sample, now containing only aerosol-free air and  $^{222}\text{Rn}$  gas, enters the main delay volume (1500 L) where  $^{222}\text{Rn}$  decay produces new progeny. The newly formed  $^{218}\text{Po}$  and  $^{214}\text{Po}$  are then collected on a second filter and their subsequent  $\alpha$  decays are counted with a ZnS photomultiplier system. Atmospheric  $^{222}\text{Rn}$  activity concentrations are then calculated from the  $\alpha$  count rate and the flow rate through the chamber.

The detection limit ( $L_D$ ) of two-filter detectors is directly related to the volume of the main delay chamber. Here,  $L_D$  is understood to represent the ambient radon concentration at which the estimated counting error of the instrument reaches 30 %. The  $L_D$  of the 1500 L model used in this study was around  $0.03\text{ Bq m}^{-3}$ . Under normal operation ANSTO monitors are automatically calibrated in situ every month by injecting radon into the sampling air stream from a well-characterized Pylon  $^{226}\text{Ra}$  source (ca. 41 kBq radium at SAC station) for 5 h at a fixed flow rate of  $\sim 100\text{ cc min}^{-1}$ . Automatic instrumental background checks, each lasting 24 h, are also performed every 3 months to keep track of long-lived  $^{210}\text{Pb}$  accumulation on the detectors' second filter (which should be changed every 5 years). Based on a calibration source uncertainty of 4 %, coefficient of variability of valid monthly calibrations of 2 %–6 %, and counting uncertainty of around 2 % for radon concentrations  $\geq 1\text{ Bq m}^{-3}$ , the total measurement uncertainty of 1500 L ANSTO radon detectors is typically between 8 % and 12 % ( $k = 2$ ). The ANSTO monitors have low maintenance requirements, but due to their dimensions (2.5–3 m long) it can be challenging to in-

**Table 1.** Summary of principal characteristics of the  $^{222}\text{Rn}$  and  $^{222}\text{Rn}$  progeny monitors compared in the present study.

Monitor	Method	Sampling flow rate ( $\text{L min}^{-1}$ )	$L_D$ ( $\text{Bq m}^{-3}$ )	Typical uncertainty ( $k = 2$ )	Portability considerations, dimensions ( $\text{cm} \times \text{cm} \times \text{cm}$ ), and weight (kg)	Deployability	References
ANSTO	Dual flow loop, two filters	$\sim 83$	$\sim 0.03$	$< 12\%$	$300 \times 80 \times 80$ $\sim 120$	- Remote control - Time response correction - Need of large pump if the simple intake line is more than $\sim 10$ m in length	Whittlestone and Zahorowski (1998), Brunke et al. (2002), Chambers et al. (2018)
ARMON	Electrostatic deposition	$\sim 2$	$\sim 0.07$	$< 35\%$	$90 \times 80 \times 80$ $\sim 10$	- $\alpha$ Spectrum - Remote control - Need of dry air simple	Grossi et al. (2012), Vargas et al. (2015)
HRM	One filter	$\sim 20$	$\sim 0.07$	$< 15\%$	$35 \times 30 \times 15$ $\sim 8$	- $\alpha$ Spectrum - Remote control - Sampling inlet height correction	Levin et al. (2002)
LSCE	One filter	$\sim 160$	$\sim 0.01$	$< 20\%$	$25 \times 25 \times 40$ $\sim 8$	- $\alpha$ Spectrum - Remote control - Sampling inlet height correction - Need of large pump	Polian (1986), Biraud (2000)

stall them at stations with space restrictions. As an alternative to the 1500 L detectors, a 700 L model is also available, which is more portable and has a  $L_D$  of  $0.04\text{--}0.05 \text{ Bq m}^{-3}$ . The combination of detector volume, operating flow rate, and radon decay chain results in ANSTO monitors having a response time of  $\sim 45$  min, which can be corrected for in post-processing (Griffiths et al., 2016).

Two ANSTO monitors were used during this study. As explained later in the text these monitors are permanently running at SAC and ODM stations. No calibration source was available when the ANSTO monitor was installed at the ODM site, so calibration and background information derived prior to transport have been used.

### Electrostatic deposition monitor

The atmospheric radon monitor (ARMON) used in this experiment was designed and built at the Institut de Tècniques Energètiques (INTE) of the UPC. The ARMON is a portable instrument based on the electrostatic deposition method, consisting of alpha spectrometry of positive ions of  $^{218}\text{Po}$  electrostatically collected on a detector (Hopke, 1989; Pereira and da Silva, 1989; Tositti et al., 2002). The ARMON is described in detail in Grossi et al. (2012).

Sampled air with a flow rate between 1 and  $2 \text{ L min}^{-1}$  is first filtered to remove ambient  $^{222}\text{Rn}$  and  $^{220}\text{Rn}$  progeny and then pumped through a  $\sim 20$  L spherical detection volume uniformly covered internally with silver. Within this volume the newly formed  $^{222}\text{Rn}$  and  $^{220}\text{Rn}$  progeny, i.e., positive

$^{218}\text{Po}$  and  $^{216}\text{Po}$  ions, respectively, are electrostatically collected on a passivated implanted planar silicon (PIPS) detector surface by an electrostatic field inside the spherical volume. An 8 kV potential is applied between the PIPS detector base and the sphere walls. As for the ANSTO detector, the sensitivity of this instrument type depends on the detector volume. The design of the monitor employed in this study has a  $L_D$  of about  $0.07 \text{ Bq m}^{-3}$  in agreement with the definition given above. Grossi et al. (2012) reported a minimum detection limit for this instrument of around  $0.2 \text{ Bq m}^{-3}$  in agreement with the definition of Gilmore (2008). The measurement efficiency of the electrodeposition method is reduced due to neutralization of the positive  $^{218}\text{Po}$  in recombination with  $\text{OH}^-$  ions in the sampled air (Hopke, 1989). Consequently, it is necessary to dry the sampled air as much as possible before it enters the detection volume. To this end, a dew point of  $< -40^\circ\text{C}$  was maintained at both intercomparison sites using a cryocooler, consisting of a vessel tube where sampling air was passing through before reaching the radon monitor (Grossi et al., 2018).

Each ARMON is calibrated at the INTE-UPC  $^{222}\text{Rn}$  chamber (Vargas et al., 2004) under different  $^{222}\text{Rn}$  and relative humidity conditions (Grossi et al., 2012). The radon chamber of the INTE-UPC is a  $20 \text{ m}^3$  installation, which allows control of the exhalation rate ( $0\text{--}256 \text{ Bq min}^{-1}$ ) and the ventilation air flow rate ( $0\text{--}100 \text{ L min}^{-1}$ ). The  $^{222}\text{Rn}$  source is a dry powder material containing  $2100 \text{ kBq } ^{226}\text{Ra}$  activity enclosed in the source container (RN-1025 model manufactured by Pylon Electronics). The calibration factor  $F_{\text{cal}}$  of

the ARMON used in this study was 0.39 counts per minute (cpm) per becquerel per cubic meter with an uncertainty of 10 % ( $k = 2$ ). The correction factor for the humidity influence inside the sphere was  $6.5 \times 10^{-5}$  per part per million  $\text{H}_2\text{O}$  (ppm) with a maximum uncertainty of 10 % ( $k = 2$ ). The total uncertainty of the atmospheric radon activity concentration measured by the ARMON is about 20 % ( $k = 2$ ) for atmospheric  $^{222}\text{Rn}$  levels in the range of a few hundred becquerels per cubic meter but could increase up to 30 %–35 % ( $k = 2$ ) when atmospheric  $^{222}\text{Rn}$  levels decrease to a few becquerels per cubic meter due to the increase in the error of the alpha counts. The total uncertainty includes the calibration factor  $F_{\text{cal}}$ , the background due to the presence of  $^{212}\text{Po}$  from  $^{220}\text{Rn}$ , the net  $^{218}\text{Po}$  counts, and the humidity correction factor (Grossi et al., 2012; Vargas et al., 2015). Every 1–2 years the progeny filter at the ARMON inlet should be changed. The detection volume of the ARMON is safely isolated because it is located within an external wooden cube of  $0.18 \text{ m}^3$ .

### 2.1.2 Indirect methods

#### One-filter monitors

One-filter detectors measure the decay rates of aerosol-bound  $^{222}\text{Rn}$  progeny directly accumulated by air filtration (Schmithüsen et al., 2017). The  $^{222}\text{Rn}$  activity concentration is then calculated assuming a constant disequilibrium factor ( $F_{\text{eq}}$ ) for a given site and sampling height between  $^{222}\text{Rn}$  and the measured progeny in the sampled air.

In the present study two monitors based on this method were used. One, named HRM here, was developed at the Institute of Environmental Physics of Heidelberg University, Germany, and is described in detail by Levin et al. (2002). Rosenfeld (2010) describe the most recent version of this monitor for which the electronics, data acquisition, and evaluation hardware and software were modernized. The HRM measurement is based on  $\alpha$  spectrometry of  $^{222}\text{Rn}$  daughters attached to atmospheric aerosols collected on a static quartz fiber filter (QMA  $\varnothing 47 \text{ mm}$ ) using a surface barrier detector (Canberra CAM 900  $\text{mm}^2$  active surface). The  $L_D$  of the HRM is about  $0.07 \text{ Bq m}^{-3}$  at a flow rate of about  $20 \text{ L min}^{-1}$  with an uncertainty smaller than 15 % ( $k = 2$ ) for atmospheric  $^{222}\text{Rn}$  levels above  $2 \text{ Bq m}^{-3}$ . This includes the uncertainty of the line loss correction (see below). Since one-filter detectors have no need for any delay chambers but use only a compact filter holder with an integrated detector and pre-amplifier, the HRM is a small instrument with high portability. Regarding maintenance requirements, the quartz fiber filter should be changed monthly.

During the measurement campaign carried out at the Saclay station, where air samples were collected via a 100 m Decabon tubing (see below), the line loss correction of Levin et al. (2017) was applied to all data of the HRM. No loss of aerosol was assumed in the short tubing used at Orme

de Mérisiers station. Here we report  $^{214}\text{Po}$  activity concentrations for both sites. However, for the 100 m intake height at Saclay we would not expect any disequilibrium, meaning that, based on the results from Schmithüsen et al. (2017), the reported  $^{214}\text{Po}$  activity concentrations directly correspond to  $^{222}\text{Rn}$  activity concentrations. By contrast, for the 2 m intake height at ODM we expect a  $^{214}\text{Po}/^{222}\text{Rn}$  disequilibrium of about 0.85 to 0.9.

The second type of one-filter monitor participating in this study was built at the Laboratoire des Sciences du Climat et de l'Environnement, LSCE, France (Polian, 1986; Biraud, 2000; Schmithüsen et al., 2017). Within this paper this monitor will be called the LSCE monitor. This monitor uses a moving filter band system, which allows the determination of atmospheric  $^{222}\text{Rn}$  activity concentration based on measurements of its progeny  $^{218}\text{Po}$  and  $^{214}\text{Po}$ . Attached  $^{222}\text{Rn}$  progeny are collected on a cellulose filter (Pöllman-Schneider) over a 1 h period at a flow rate of  $160 \text{ L min}^{-1}$  and after this aerosol sampling period, the loaded filter is moved to the  $\alpha$  spectrometry for a 1 h measurement period by a scintillator from Harshaw Company Co. and photomultiplier from EMI Electronics Ltd. (Biraud, 2000). The  $L_D$  is about  $0.01 \text{ Bq m}^{-3}$  with an uncertainty of about 20 %.

Regarding maintenance on a regular basis, the LSCE monitor's filter roll has to be changed every 3 weeks. Automatic detector background is performed every 3 weeks, and counting efficiency is manually tested with an americium source. The instrument is designed to measure radioactive aerosols a few meters above the ground level. An inlet filter is installed to block black carbon or dirt deposition when the instrument is installed in urban areas as the flow rate drops below  $9 \text{ m}^3 \text{ h}^{-1}$ . The instrument is about 25 cm high, 40 cm long, and 25 cm deep, and it can be easily deployed at a station.

### 2.2 Sites

The present intercomparison study was carried out at two stations located 30 km southwest of Paris in the fall and winter of 2016–2017 (Fig. 1). Both stations, 3.5 km apart, belong to the LSCE and are located in a region with a radon flux of ca.  $5\text{--}10 \text{ mBq m}^{-2} \text{ s}^{-1}$  in winter, according to output of the Karsten et al. (2015) model.

Phase I of the measurements started at Orme des Mérisiers (ODM, latitude 48.698, longitude 2.146, 167 m above sea level) and ran between 25 November 2016 and 23 January 2017. Here, LSCE and ANSTO (for convenience named ANSTO\_ODM here) monitors are routinely running. During Phase I of the intercomparison exercise these two monitors were operated in parallel with a HRM and an ARMON. The sampling height for all radon detectors at ODM was 2 m a.g.l.

Phase II of the exercise was realized at Saclay (SAC, latitude 48.730, longitude 2.180; Fig. 1) between 25 January and 13 February 2017. At this location the sampling inlet height was at 100 m a.g.l. At SAC station another ANSTO monitor

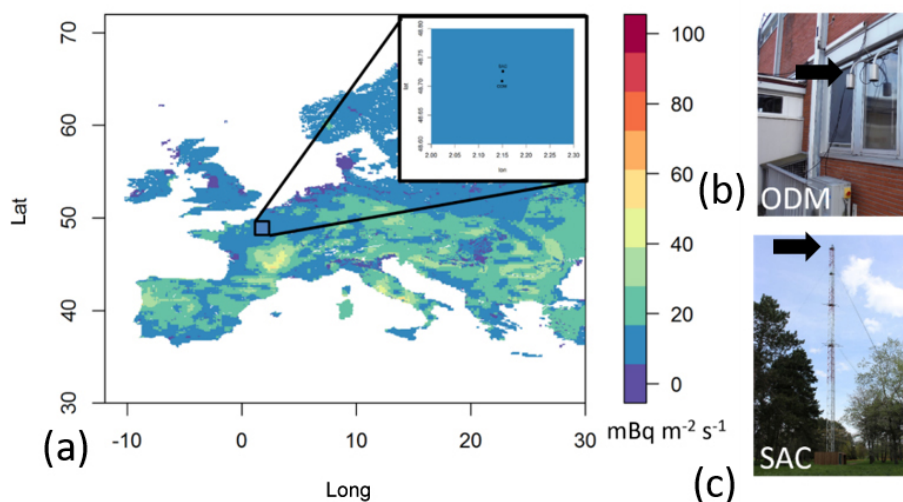


**Figure 1.** The INGOSv2.0  $^{222}\text{Rn}$  flux map (Karstens et al., 2015) is shown for a typical winter month (December), with locations of the ODM and SAC sites shown in the inset in (a). The radon sampling inlets are indicated for both ODM (b) and SAC (c) by the black arrows.

(from now on labeled ANSTO\_SAC) was already running. In addition, during Phase II this detector was running in parallel with the portable ARMON and HRM detectors. The LSCE monitor did not participate in Phase II of the experiment.

Meteorological parameters were also available at both stations during the intercomparison periods at heights corresponding to the radon measurements (2 and 100 m a.g.l.). In the case of the ODM site, atmospheric aerosol concentrations were also measured for this period.

### 2.3 Environmental parameters and atmospheric aerosol concentration

Meteorological data used within this study were available from continuous measurements carried out at the SAC and ODM stations at 100 m and at 10 m a.g.l., respectively. The measurements were performed with a Vaisala weather transmitter WXT520 (Campbell Scientific) for (1) wind speed and direction (accuracies of  $\pm 3\%$  and  $\pm 3^\circ\text{C}$ , respectively) and (2) humidity and temperature (accuracies of  $\pm 3\%$  and  $\pm 0.3^\circ\text{C}$ , respectively). In addition, the atmospheric aerosol concentration was measured at the ODM site using a fine dust measurement device Fidas<sup>®</sup> 200 S (Palas) at 10 m a.g.l. The measurement range is between 0 and 20 000 particles  $\text{cm}^{-3}$ . All the accuracies refer to the manufacturer's specifications.

### 2.4 Data analysis

#### 2.4.1 Correlation factors between monitors

To study the correlation between responses of the different detectors, linear regression models were calculated using hourly atmospheric radon activity concentrations from each monitor. The linear regression fits were calculated following Krystek and Anton (2007), relative to the two portable detec-

tors, ARMON and HRM, because they both were measuring at SAC and at ODM.

#### 2.4.2 Analysis of the influence of the environmental and meteorological parameters on detector response

The present study intended to build upon the findings of Xia et al. (2010) and Schmithüsen et al. (2017) regarding the possible influence of meteorological conditions on the response of radon and radon progeny monitors.

With this in mind, the ratio between hourly atmospheric  $^{222}\text{Rn}$  activity concentrations measured and/or obtained by the HRM, LSCE, and ANSTO monitors and that measured by the ARMON were calculated, and their variability was analyzed in relation to hourly atmospheric temperature, relative humidity, and atmospheric aerosol concentration measured at ODM and at SAC. Not enough rain data were available to be used in this study. For this part of the study, the ARMON was used as a reference since it was the only direct radon monitor running at both sites.

## 3 Results

Hourly time series of atmospheric  $^{222}\text{Rn}$ , in the case of the ARMON and ANSTO monitors, and  $^{222}\text{Rn}$  progeny ( $^{214}\text{Po}$  activity concentration) for the HRM and LSCE monitors, measured at ODM and SAC during Phase I and Phase II of the intercomparison experiment, are presented in Figs. 2 and 3, respectively. In each of the previous figures, a zoom plot has also been reported as an example of the response of each monitor to the sub-diurnal atmospheric radon variability. As shown, all monitors running at both sites follow this variability, with  $^{222}\text{Rn}$  and  $^{222}\text{Rn}$  progeny data measured or estimated by the three different measurement tech-

niques showing the same general patterns. Table 2 summarizes the mean, minimum, and maximum hourly atmospheric radon or radon progeny activity concentrations measured by each monitor for both campaigns. For further information, Figs. S1 and S2 in the Supplement show the time series of the differences (absolute) and of the ratios (relative) between the hourly  $^{214}\text{Po}$  or  $^{222}\text{Rn}$  activity concentrations measured by HRM, LSCE, and ANSTO monitors and those measured by the ARMON.

### 3.1 Phase I: ODM site

During Phase I the LSCE, HRM, ARMON, and ANSTO\_ODM monitors were operating in parallel, sampling air from the same height (2 m a.g.l.). The mean temperature over Phase I of the campaign was  $2.9^\circ\text{C}$  with an interquartile range of  $0.10$  to  $5.8^\circ\text{C}$ . The mean relative humidity was 80 % with an interquartile range of 73 % to 89 %. An average accumulated rain per day of 13 mm was recorded. The main wind patterns during Phase I were from the northeast and southwest, with speeds typically between 1 and  $7\text{ m s}^{-1}$ . The mean atmospheric aerosol concentration observed at ODM during Phase I was  $505\text{ particles cm}^{-3}$  with an interquartile range of 233 to  $660\text{ cm}^{-3}$ .

The means of the atmospheric  $^{222}\text{Rn}$  activity concentration measured by the ARMON and the ANSTO\_ODM are in the same order (Table 2). The means of the atmospheric  $^{214}\text{Po}$  activity concentrations measured by the LSCE monitor were ca. 50 % lower and ca. 30 % lower by the HRM than the atmospheric  $^{222}\text{Rn}$  activity concentration.

Table 2 shows the slopes ( $b$ ) and intercepts ( $a$ ) of the linear regression fits calculated between the hourly atmospheric  $^{222}\text{Rn}$  and  $^{214}\text{Po}$  activity concentrations measured by the ARMON and/or the HRM and the other  $^{222}\text{Rn}$  and  $^{222}\text{Rn}$  progeny monitors deployed in Phase I. The calculated slopes were in the range of 0.62 to 1.17, and the  $R^2$  values varied between 0.90 and 0.96. The slope closest to unity was calculated between the ARMON and ANSTO\_ODM monitors and was  $0.96 \pm 0.01$ , while the lowest slope was observed between the ARMON and LSCE monitors and was  $0.62 \pm 0.01$ . The highest correlation ( $R^2 = 0.96$ ) was found between the HRM and LSCE monitors. The plots of the linear regression fits of Phase I are shown in the left panels of Figs. S3, S4, and S5. Notably, the offset ( $a$  value) of the regression between the ANSTO and ARMON detectors at ODM is considerably greater than that at SAC. The regression slopes are also slightly different. These differences are likely related to the limited calibration and background information available for the ANSTO\_ODM detector for this intercomparison project. In particular, a substantial component of the instrumental background signal is site specific. This is likely responsible for much of the change in offset value.

### 3.2 Phase II: SAC station

Phase II lasted 18 d. The mean temperature during this period was  $5^\circ\text{C}$  with an interquartile range of 2 to  $8^\circ\text{C}$ . The mean relative humidity was 86 % with an interquartile range of 80 % to 94 %. An average accumulated rain per day of 3 mm was recorded. The main wind patterns during this phase at 100 m a.g.l. were from the south and southwest with speeds typically between 3 and  $10\text{ m s}^{-1}$ .

Figure 3 shows the hourly atmospheric  $^{222}\text{Rn}$  and  $^{214}\text{Po}$  activity concentrations observed at SAC during Phase II by the ARMON, HRM, and ANSTO\_SAC instruments.

Table 2 reports the means, minima, and maxima of the atmospheric data measured during Phase II by all participating monitors. In this case, the mean atmospheric  $^{222}\text{Rn}$  and  $^{214}\text{Po}$  activity concentrations measured by all monitors agreed within the instrumental errors. At 100 m a.g.l. the slopes of the hourly fits of the monitor's response in this case were all close to unity. The calculated offsets also decreased at 100 m a.g.l. relative to 2 m a.g.l. The plots of the linear regression fits of Phase II are shown in the right panel of Figs. S5 and S6. During the period of 30 January to 1 February 2019, the HRM shows significantly lower values than ANSTO and ARMON. This period coincides with saturated air humidity conditions.

Figure S7 presents two plots to summarize the results of the slopes and offsets calculated at both ODM and SAC stations relative to the ARMON.

Figures 2 and 3 show a larger hourly variability of the HRM and ARMON signals compared with the ANSTO ones. This difference in variability is likely due to a larger uncertainty of the HRM and ARMON detectors for atmospheric  $^{222}\text{Rn}$  levels of around  $1\text{ Bq m}^{-3}$ . In addition, it has to be taken into account that only an approximated form of the Griffiths et al. (2016) response time correction could be applied to the output of the ANSTO detectors. Further investigations should be carried out to clarify these differences and to exactly quantify the detectors' uncertainties for the low  $^{222}\text{Rn}$  concentrations typical for outdoor environmental monitoring at or above 100 m a.g.l.

### 3.3 Comparison with past studies

The results obtained in the present study of the slopes ( $b$ ) and of the offsets ( $a$ ) of the regression lines calculated between ANSTO or LSCE monitors against the HRM are here compared with the ones presented by Schmithüsen et al. (2017). Table 3 shows a summary of this comparison. All slopes (correction factors) are defined as (routine station monitor) divided by HRM because this last was used as the reference instrument by Schmithüsen et al. (2017).

Data in Table 3 need to be analyzed taking into account that a unique traceability chain is not yet available for atmospheric radon measurements and the different monitors routinely running at the different stations could have differ-



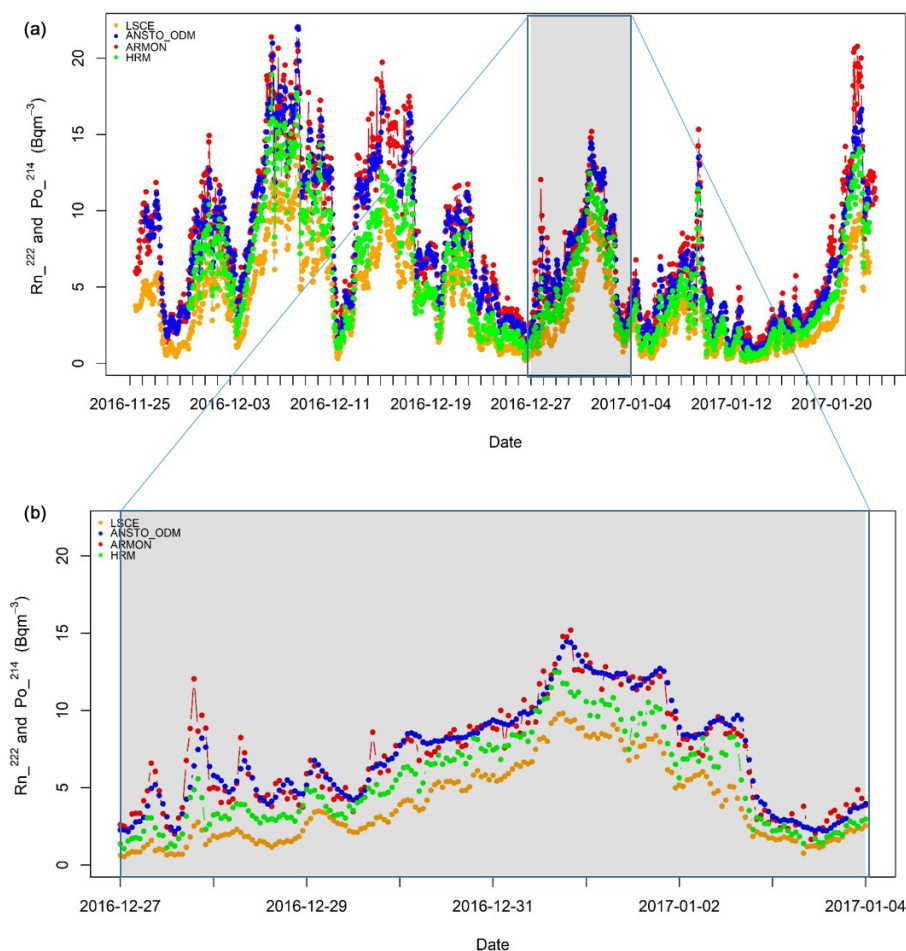


**Figure 2.** (a) Hourly time series of the atmospheric  $^{222}\text{Rn}$  and, in the case of LSCE and HRM data,  $^{214}\text{Po}$  activity concentration, measured at the Orme de Mérisiers (ODM) station during Phase I (between 25 November 2016 and 23 January 2017) by the ARMON (red circles), ANSTO\_ODM (blue circles), HRM (green circles), and LSCE (orange circles) monitors. (b) Hourly time series of the atmospheric  $^{222}\text{Rn}$  and  $^{214}\text{Po}$  measured between 27 December 2016 and 4 January 2017.

ent calibration chains (e.g., radon source, primary standard). Generally speaking, for both studies, it can be observed that the correction factor between the atmospheric  $^{214}\text{Po}$  activity concentration measured by HRM and the atmospheric  $^{222}\text{Rn}$  activity concentration measured by ANSTO at each station approaches unity with the increase in the height of the sampling input. By contrast, the offsets of the regression fits decrease with the increase in the input height.

The only case where the compared instruments were exactly the same and at the same height is for the Orme des Mérisiers station. Here the slope between the atmospheric  $^{214}\text{Po}$  activity concentration measured by LSCE and HRM is equal to  $0.76 \pm 0.01$ . This number is slightly larger but within uncertainties comparable to the number reported by Schmithüsen et al. (2017) of  $0.68 \pm 0.03$  (see Table 3).

### 3.4 Influence of the weather conditions on the ratio between $^{214}\text{Po}$ and $^{222}\text{Rn}$ measurements

Figure 4 shows the variability of the ratio between hourly atmospheric  $^{214}\text{Po}$  and/or  $^{222}\text{Rn}$  activity concentration measured by each monitor relative to those measured by the ARMON versus the hourly means of ambient temperature and relative humidity. Analysis was carried out at ODM (Fig. 4a, b) and at SAC (Fig. 4c, d) versus ambient temperature (Fig. 4, left panels) and relative humidity (Fig. 4b, d) measured at the corresponding stations.

Figure 5 shows the same variability plotted in relation to the ANSTO\_ODM at ODM (Fig. 5a, b) and to the ANSTO\_SAC at SAC (Fig. 5c, d) versus the hourly means of ambient temperature (Fig. 5a, c) and relative humidity (Fig. 5b, d).

Data do not show any evident patterns at 100 m a.g.l. (SAC station), which could indicate that there is not any impact

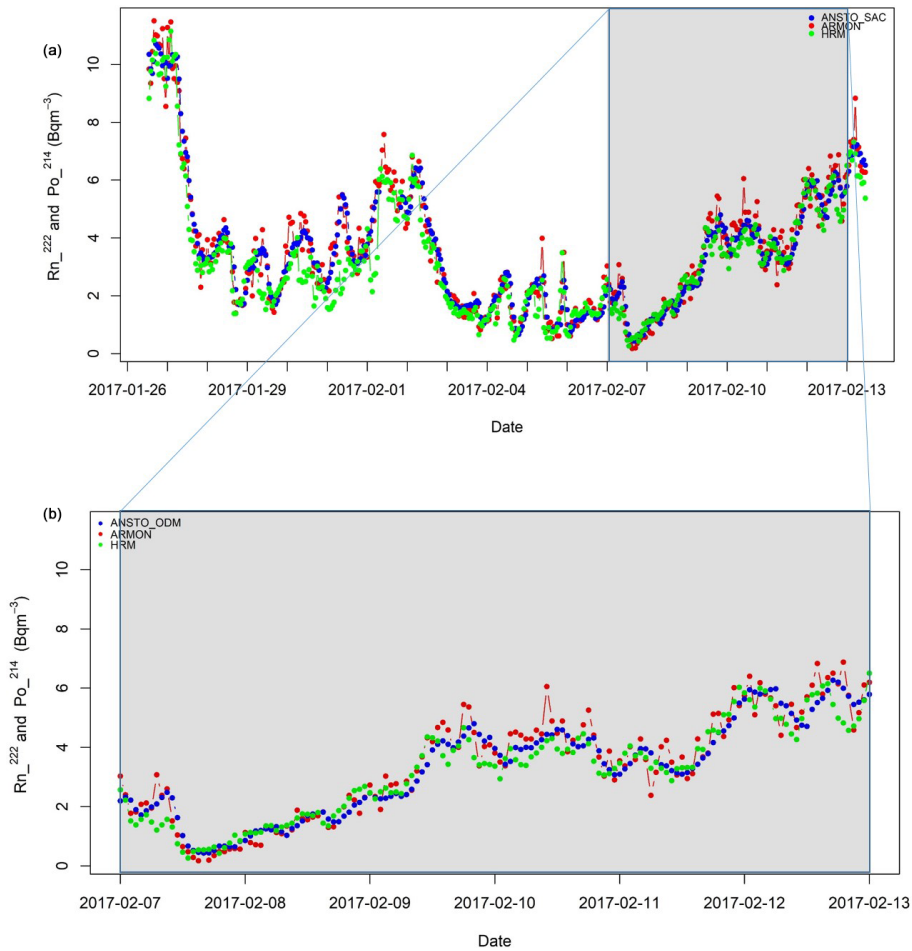


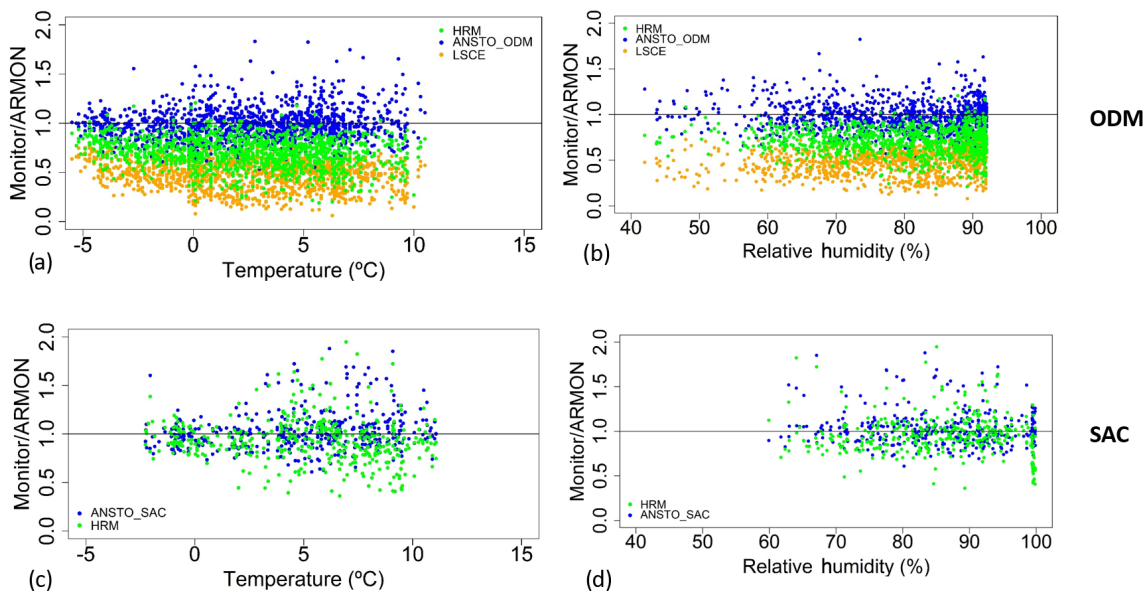
**Figure 3.** (a) Hourly time series of the atmospheric  $^{222}\text{Rn}$  and  $^{214}\text{Po}$  (HRM) activity concentration measured at the Saclay (SAC) station between 25 January and 13 February 2017 by the ARMON (red circles), ANSTO\_SAC (blue circles), and HRM (green circles) monitors. (b) Hourly time series of the atmospheric  $^{222}\text{Rn}$  and  $^{214}\text{Po}$  measured between 7 and 13 February 2017.

**Table 2.** The means, maxima, and minima of the atmospheric  $^{222}\text{Rn}$  and  $^{214}\text{Po}$  activity concentration observed by each monitor participating in Phases I and II of the intercomparison campaigns. The slopes ( $b$ ) and intercepts ( $a$ ) of the linear regression fits calculated between the hourly atmospheric  $^{222}\text{Rn}$  and  $^{214}\text{Po}$  activity concentrations measured by the ARMON and/or the HRM and the other  $^{222}\text{Rn}$  and  $^{222}\text{Rn}$  progeny monitors deployed in both phases are also reported.

Monitors Phase I	Mean ( $\text{Bq m}^{-3}$ )	Min/max ( $\text{Bq m}^{-3}$ )	$x$					
			$b$ (ARMON)	$a$ (ARMON)	$R^2$ (ARMON)	$b$ (HRM)	$a$ (HRM)	$R^2$ (HRM)
ANSTO_ODM	7.02	0.73/22.04	$0.96 \pm 0.01$	$-0.23 \pm 0.03$	0.94	$1.17 \pm 0.01$	$0.63 \pm 0.03$	0.93
HRM	5.45	0.26/18.91	$0.82 \pm 0.01$	$-0.71 \pm 0.03$	0.93	–	–	–
ARMON	7.55	0.50/21.98	–	–	–	–	–	–
LSCE	3.84	0.10/14.93	$0.62 \pm 0.01$	$-0.85 \pm 0.03$	0.90	$0.76 \pm 0.004$	$-0.29 \pm 0.03$	0.96
$y$ Monitors Phase II	Mean ( $\text{Bq m}^{-3}$ )	Min/max ( $\text{Bq m}^{-3}$ )	Slope (ARMON)	Intercept (ARMON)	$R^2$ (ARMON)	Slope (HRM)	Intercept (HRM)	$R^2$ (HRM)
ANSTO_SAC	3.50	0.43/10.71	$0.97 \pm 0.01$	$0.01 \pm 0.06$	0.95	$1.03 \pm 0.01$	$0.15 \pm 0.06$	0.90
HRM	3.26	0.26/11.15	$0.94 \pm 0.01$	$-0.13 \pm 0.06$	0.91	–	–	–
ARMON	3.60	0.17/11.51	–	–	–	–	–	–

**Table 3.** Offsets and slopes of the regression lines calculated between ANSTO or LSCE monitors against the HRM in the present study and by Schmithüsen et al. (2017).

Site/input height	Schmithüsen et al. (2017)			Present study		
ANSTO/HRM	Activity range ( $\text{Bq m}^{-3}$ )	$b$	$a$	Activity range ( $\text{Bq m}^{-3}$ )	$b$	$a$
Cabauw: 200/180 m	0–8	$1.11 \pm 0.04$	$0.11 \pm 0.06$	0–11	$1.03 \pm 0.01$	$0.15 \pm 0.06$
Saclay: 100 m						
Lutjewad: 60 m	0–6	$1.11 \pm 0.02$	$0.11 \pm 0.02$			
Heidelberg: 35 m	0–15	$1.22 \pm 0.01$	$0.42 \pm 0.04$			
Cabauw: 20 m	0–12	$1.30 \pm 0.01$	$0.21 \pm 0.03$			
Orme des Mérisiers: 2 m				0–22	$1.17 \pm 0.01$	$0.63 \pm 0.03$
LSCE/HRM	Activity range ( $\text{Bq m}^{-3}$ )	$b$	$a$	Activity range ( $\text{Bq m}^{-3}$ )	$b$	$a$
Orme des Mérisiers: 2 m	0–9	$0.68 \pm 0.03$	$-0.18 \pm 0.09$	0–15	$0.76 \pm 0.01$	$-0.29 \pm 0.03$

**Figure 4.** Hourly atmospheric  $^{222}\text{Rn}$  or  $^{214}\text{Po}$  activity concentration obtained by the HRM, LSCE, and ANSTO monitors divided by the  $^{222}\text{Rn}$  activity concentration measured by the ARMON detector as a function of the hourly measured atmospheric temperature and relative humidity at ODM (a, b) and at SAC (c, d).

on  $^{222}\text{Rn}$  or  $^{222}\text{Rn}$  progeny measurements due to change in ambient temperature and relative humidity, at least not until saturated conditions are achieved. By contrast, a small decrease, of about  $10^{-2} \text{ } ^\circ\text{C}^{-1}$ , is observed in the ratio between the  $^{214}\text{Po}$  activity concentration (measured by the HRM and LSCE monitors) and the  $^{222}\text{Rn}$  activity concentration (measured by the ANSTO\_ODM and ARMON monitors) with the increase in the ambient temperature (Fig. S8) at 2 m a.g.l. (ODM station). This temperature dependency may be rather due to the effect of atmospheric activity concentrations, increasing during nighttime, on the disequilibrium between radon and its progeny. However, this influence on measured  $^{214}\text{Po}/^{222}\text{Rn}$  ratios is really small compared with

other observed effects (e.g., loss of progeny within the sample tube (Levin et al., 2017) or atmospheric aerosol concentration; see below). Looking at Fig. 5, there appears to be less scatter in the point clouds (particularly at SAC) when the ANSTO\_SAC monitor is used as the reference, likely attributable to the lower measurement uncertainty of the ANSTO monitor used at this station.

In Fig. 6 the ratio of the hourly atmospheric  $^{222}\text{Rn}$  or  $^{222}\text{Rn}$  progeny activity concentration measured by the HRM ( $^{214}\text{Po}$  in Fig. 6a), the LSCE ( $^{214}\text{Po}$  in Fig. 6b), and the ANSTO\_ODM ( $^{222}\text{Rn}$  in Fig. 6c) monitors and the  $^{222}\text{Rn}$  activity concentration measured with ARMON ( $^{222}\text{Rn}$ ) are plotted against the logarithm of the hourly aerosol concentra-

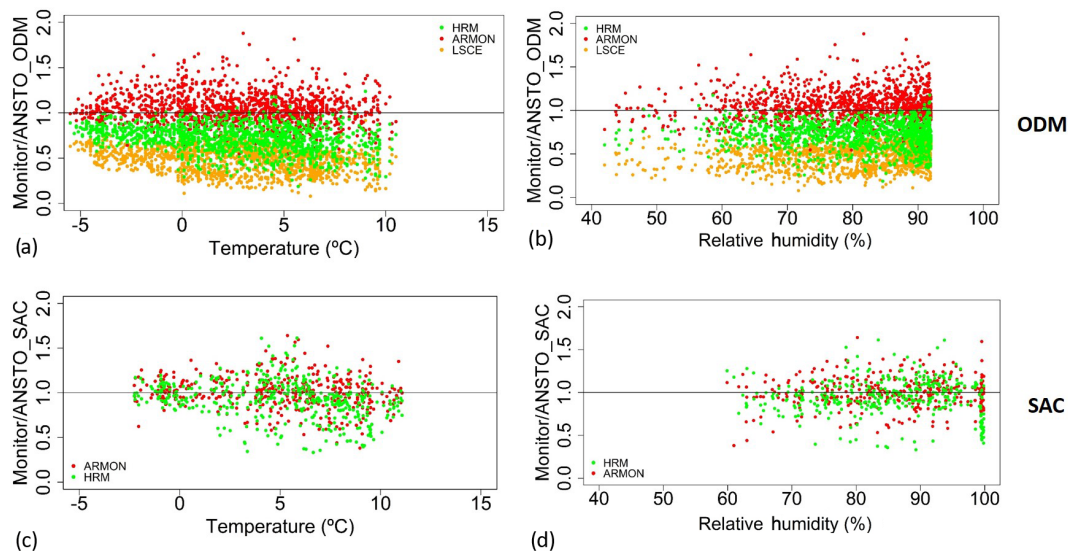


**Figure 5.** Hourly atmospheric  $^{222}\text{Rn}$  or  $^{214}\text{Po}$  activity concentration obtained by ARMON, HRM, and LSCE monitors divided by the  $^{222}\text{Rn}$  activity concentration measured by the ANSTO detectors as a function of the hourly measured atmospheric temperature and relative humidity at ODM (a, b) and at SAC (c, d).

tion data. Data indicate the existence of a linear relationship between these variables, i.e., of the form

$$\frac{^{222}\text{Rn}(\text{Monitor}_i)}{^{222}\text{Rn}(\text{ARMON})} = a + b \cdot \text{Log}_{10}(\text{aerosol conc.}). \quad (1)$$

Here  $^{222}\text{Rn}(\text{Monitor}_i)$  is the hourly atmospheric  $^{222}\text{Rn}$  or  $^{214}\text{Po}$  activity concentration measured by individual monitors HRM ( $^{214}\text{Po}$ ), LSCE ( $^{214}\text{Po}$ ), and ANSTO\_ODM ( $^{222}\text{Rn}$ );  $^{222}\text{Rn}(\text{ARMON})$  is the one measured by the ARMON monitor; and aerosol conc. is the hourly atmospheric aerosol concentration measured at ODM during Phase I. The results of the linear regression fits are reported in Table 4. The slope of the ratio between the ANSTO\_ODM and ARMON monitors in relation to the variability of the logarithm of the hourly atmospheric aerosol concentration is close to zero, and the intercept is close to 1. The ratio between the hourly atmospheric aerosol-bound radon progeny data measured by the two one-filter radon progeny monitors and the one measured by the ARMON seems to decrease with decreasing aerosol concentration (Fig. 6a and b). However, this effect only becomes evident when atmospheric aerosol concentration is lower than  $300 \text{ particles cm}^{-3}$ .

#### 4 Conclusions

In order to confirm and build upon the results obtained by Xia et al. (2010), Grossi et al. (2016), and Schmithüsen et al. (2017), a 3-month intercomparison campaign was carried out in the south of Paris, France, in the fall–winter period of 2016–2017. For the first time, three fundamentally distinct radon and radon progeny measurement approaches were

**Table 4.** Intercepts and slopes of the linear regression fits of the Eq. (1).

Monitor	$a$	$b$	$R^2$
HRM	$0.10 \pm 0.02$	$0.23 \pm 0.01$	0.34
LSCE	$-0.07 \pm 0.02$	$0.21 \pm 0.01$	0.34
ANSTO_ODM	$0.91 \pm 0.03$	$0.03 \pm 0.01$	$0.04 \times 10^{-1}$

compared side by side at two measurement heights, 2 and 100 m a.g.l., under a range of environmental conditions with the aim to compare their responses.

The results of this study show that  $^{222}\text{Rn}$  and  $^{222}\text{Rn}$  progeny measurements follow the same general patterns of diurnal variability, both close to and further up from the surface. The slopes of the linear regression fits between the radon and the radon progeny measurements, which represent the calibration factors, are not significantly different from one at 100 m height above ground (SAC), but they differ at the 2 m level (ODM). The latter is attributable to the disequilibrium known to exist between  $^{222}\text{Rn}$  freshly emitted from the ground and its short-lived progeny in the lowest tens of meters of the atmosphere, the magnitude of which is known to decrease with distance from the surface, as shown in earlier work, and to be close to 1 at a height of 100 m and above (e.g., Jacobi and André, 1963; Schmithüsen et al., 2017).

For the 2 m level, we found a significant correlation of radon progeny activity concentrations between LSCE and HRM measurements (see Fig. S3). The slope, however, is only equal to  $0.76 \pm 0.01$ . This result is comparable, considering its uncertainties, with the result reported by Schmithüsen



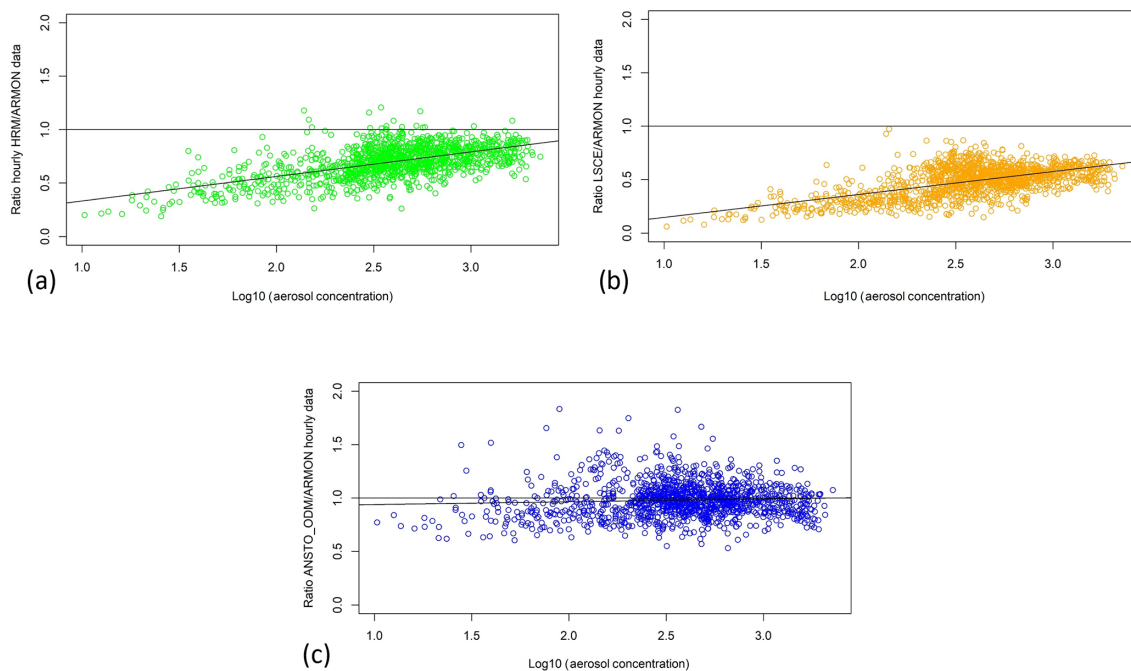


**Figure 6.** Ratio of the atmospheric  $^{222}\text{Rn}$  or  $^{214}\text{Po}$  activity concentration measured by the HRM (green dots), LSCE (orange dots), and ANSTO\_ODM (blue dots) monitors and those measured by the reference ARMON monitor against the logarithm of the atmospheric aerosol concentration measured at the ODM station.

et al. (2017) of  $0.68 \pm 0.03$  (see Table 3) based on the comparison of the same two monitors (HRM and LSCE) and at the same station (ODM) in March and April 2014.

Observations of the total atmospheric aerosol concentration available at the ODM station during the first 2 months of the experiment were used to investigate the influence of changing atmospheric aerosol concentrations on the response of the radon and radon progeny measurements. Under very low atmospheric aerosol loading ( $< 300$  particles  $\text{cm}^{-3}$ ), the  $^{222}\text{Rn}$  progeny monitors seem to underestimate the atmospheric  $^{214}\text{Po}$  activity concentrations by up to 50%. This effect may be attributable to loss of unattached  $^{218}\text{Po}$  and  $^{214}\text{Po}$ . Particle number concentrations below  $300$  particles  $\text{cm}^{-3}$  at continental stations are, however, very rare, and even during winter at Alpine stations like Schneefernerhaus such low particle concentrations are only occasionally observed (Birmili et al., 2009).

The comparison of results obtained in the present study with those reported in Schmithüsen et al. (2017) demonstrate that in order to harmonize atmospheric  $^{222}\text{Rn}$  activity concentrations measured at different atmospheric networks it will be important to (i) have a well-established metrological chain; (ii) have traceable methods for measuring low-level atmospheric radon activity concentrations; (iii) harmonize the calculation of total uncertainty in atmospheric  $^{222}\text{Rn}$  concentrations measured by all monitors when ambient radon is only a few becquerels per cubic meter or less and (iv) use a direct radon monitor as a mobile reference instrument, the

response of which is not influenced by meteorological conditions or inlet tube dimensions and length.

Finally, the new portable ARMON seems to have a great potential for being used at atmospheric radon stations with space restrictions. It could also be useful as a mobile reference instrument to calibrate  $^{222}\text{Rn}$  progeny instruments or fixed radon monitors. However, the total expanded uncertainty of the ARMON could increase for really low radon activity concentrations ( $< 1$  Bq  $\text{m}^{-3}$ ) and when atmospheric  $^{220}\text{Rn}$  is also present. This should be better investigated in the near future. The uncertainties related to the ANSTO detector response time correction when characteristics of the entire intake system have not been directly measured should also be investigated.

*Code and data availability.* The raw data and the R codes used for this study are available at <https://www.dropbox.com/sh/xokyu4vnt6f0gme/AABt-DxnTBbe6FFT9p4WDZWda?dl=0> (last access: 23 April 2020, Grossi, 2020).

*Supplement.* The supplement related to this article is available online at: <https://doi.org/10.5194/amt-13-2241-2020-supplement>.

*Author contributions.* CG, OL, FRV, VK, MD, RC, JAM, SDC, and AC worked on the installation of the radon and the radon progeny monitors. In addition, they were in charge of the maintenance of

the in situ and remote radon and radon progeny measurements during the 3 months of experiment. CG, OL, VK, SDC, SW, AC, and IL worked at the calculation and delivery of the radon and radon progeny time series data. MD and MR worked on the availability of the meteorological and aerosol data covering the intercomparison campaign period.

All authors collaborated on the discussion of the data results and participated in the writing of the current paper.

*Competing interests.* The authors declare that they have no conflict of interest.

*Acknowledgements.* This study was carried out under the umbrella of the Atmospheric Thematic Center (ATC) of ICOS.

The authors warmly thank (i) the INTE team, especially Vicente Blasco and Juan Antonio Romero, for their work in the building of the ARMON used in this study, and (ii) the R project (<https://www.r-project.org/>, last access: 24 April 2020) free software environment used here for statistical computing and graphics.

This paper is dedicated to Bruno Grossi, Manuel Javier Navarro Angulo, Alfredo Adán, and the whole team of the Instituto Clínic de Oftalmología (ICOF) of the Hospital of Barcelona.

*Financial support.* This research has been supported by the Ministerio Español de Economía y Competividad, Retos 2013 (2014–2016) with the MIP (Methane interchange between soil and air over the Iberian Peninsula) project (grant no. CGL2013-46186-R) and the Ministerio Español de Educación, Cultura y Deporte (grant no. CAs15/00042).

*Review statement.* This paper was edited by Tim Arnold and reviewed by Susana Barbosa and Grant Forster.

## References

- Baskaran, M.: Po-210 and Pb-210 as atmospheric tracers and global atmospheric Pb-210 fallout: a Review, *J. Environ. Radioactiv.*, 102, 500–513, <https://doi.org/10.1016/j.jenvrad.2010.10.007>, 2011.
- Baskaran, M.: Radon: A Tracer for Geological, Geophysical and Geochemical Studies, in: Springer Geochemistry, Springer International Publishing, 260 pp., <https://doi.org/10.1007/978-3-319-21329-3>, 2016.
- Biraud, S.: Vers la régionalisation des puits et sources des composés à effet de serre: analyse de la variabilité synoptique à l'observatoire de Mace Head, Irlande, PhD thesis, University of Paris VII, France, 2000.
- Birmili, W., Ries, L., Sohmer, R., Anastou, A., Sonntag, A., König, K., and Levin, I.: Fine and ultrafine aerosol particles at the GAW station Schneefernerhaus/Zugspitze, *Gefahrst. Reinhalt. L.*, 69, 31–35, 2009.
- Brunke, E.-G., Labuschagne, C., Parker, B., van der Spuy, D., and Whittlestone, W.: Cape Point GAW Station  $^{222}\text{Rn}$  detector: factors affecting sensitivity and accuracy, *Atmos. Environ.*, 36, 2257–2262, [https://doi.org/10.1016/S1352-2310\(02\)00196-6](https://doi.org/10.1016/S1352-2310(02)00196-6), 2002.
- Chambers, S. D., Williams, A. G., Zahorowski, W., Griffiths, A., and Crawford, J.: Separating remote fetch and local mixing influences on vertical radon measurements in the lower atmosphere, *Tellus B*, 63, 843–859, <https://doi.org/10.1111/j.1600-0889.2011.00565.x>, 2011.
- Chambers, S. D., Zahorowski, W., Williams, A. G., Crawford, J., and Griffiths, A. D.: Identifying tropospheric baseline air masses at Mauna Loa Observatory between 2004 and 2010 using Radon-222 and back trajectories, *J. Geophys. Res.-Atmos.*, 118, 992–1004, <https://doi.org/10.1029/2012JD018212>, 2013.
- Chambers, S. D., Hong, S.-B., Williams, A. G., Crawford, J., Griffiths, A. D., and Park, S.-J.: Characterising terrestrial influences on Antarctic air masses using Radon-222 measurements at King George Island, *Atmos. Chem. Phys.*, 14, 9903–9916, <https://doi.org/10.5194/acp-14-9903-2014>, 2014.
- Chambers, S. D., Galeriu, D., Williams, A. G., Melintescu, A., Griffiths, A. D., Crawford, J., Dyer, L., Duma, M., and Zorila, B.: Atmospheric stability effects on potential radiological releases at a nuclear research facility in Romania: Characterising the atmospheric mixing state, *J. Environ. Radioactiv.*, 154, 68–82, <https://doi.org/10.1016/j.jenvrad.2016.01.010>, 2016.
- Chambers, S. D., Preunkert, S., Weller, R., Hong, S.-B., Humphries, R. S., Tositti, L., Angot, H., Legrand, M., Williams, A. G., Griffiths, A. D., Crawford, J., Simmons, J., Choi, T. J., Krummel, P. B., Molloy, S., Loh, Z., Galbally, I., Wilson, S., Magand, O., Sprovieri, F., Pirrone, N., and Dommergue, A.: Characterizing Atmospheric Transport Pathways to Antarctica and the Remote Southern Ocean Using Radon-222, *Front. Earth Sci.*, 6, 190, <https://doi.org/10.3389/feart.2018.00190>, 2018.
- Chambers, S. D., Guérette, E.-A., Monk, K., Griffiths, A. D., Zhang, Y., Duc, H., Cope, M., Emmerson, K. M., Chang, L. T., Silver, J. D., Utembe, S., Crawford, J., Williams, A. G., and Keywood, M.: Skill-testing chemical transport models across contrasting atmospheric mixing states using Radon-222, *Atmosphere*, 10, 25, <https://doi.org/10.3390/atmos10010025>, 2019a.
- Chambers, S. D., Podstawczyńska, A., Pawlak, W., Fortuniak, K., Williams, A. G., and Griffiths, A. D.: Characterising the state of the urban surface layer using Radon-222, *J. Geophys. Res.-Atmos.*, 124, 770–788, <https://doi.org/10.1029/2018JD029507>, 2019b.
- Frank, G., Salvamoser, J., and Steinkopf, T.: Messung radioaktiver Spurenstoffe in der Atmosphäre im Rahmen des Global Atmosphere Watch Programmes der WMO, Umweltforschungsstation Schneefernerhaus, Wissenschaftliche Resultate 2011/2012, available at: [http://www.schneefernerhaus.de/fileadmin/web\\_data/bilder/pdf/UFS-Broschuere\\_2012.pdf](http://www.schneefernerhaus.de/fileadmin/web_data/bilder/pdf/UFS-Broschuere_2012.pdf), last access: 18 August 2016.
- Galmarini, S.: One year of  $^{222}\text{Rn}$  concentration in the atmospheric surface layer, *Atmos. Chem. Phys.*, 6, 2865–2886, <https://doi.org/10.5194/acp-6-2865-2006>, 2006.
- Gilmore, G.: Practical Gamma-ray Spectrometry, 2nd edn., John Wiley & Sons, Chichester, 2008.
- Griffiths, A. D., Chambers, S. D., Williams, A. G., and Werczynski, S.: Increasing the accuracy and temporal resolution of two-filter radon-222 measurements by correcting for

- the instrument response, *Atmos. Meas. Tech.*, 9, 2689–2707, <https://doi.org/10.5194/amt-9-2689-2016>, 2016.
- Grossi, C.: LSCE\_222Rn\_Intercomparison, available at <https://www.dropbox.com/sh/xokyu4vnt6f0gme/AABt-DxnTBbe6FFT9p4WDZWda?dl=0>, last access: 23 April 2020.
- Grossi, C., Vargas, A., Camacho, A., López-Coto, I., Bolívar, J. P., Xia, Y., and Conen, F.: Inter-comparison of different direct and indirect methods to determine radon flux from soil, *Radiat. Meas.*, 46, 112–118, <https://doi.org/10.1016/j.radmeas.2010.07.021>, 2011.
- Grossi, C., Arnold, D., Adame, A. J., Lopez-Coto, I., Bolivar, J. P., de la Morena, B. A., and Vargas, A.: Atmospheric  $^{222}\text{Rn}$  concentration and source term at El Arenosillo 100 m meteorological tower in southwest Spain, *Radiat. Meas.*, 47, 149–162, <https://doi.org/10.1016/j.radmeas.2011.11.006>, 2012.
- Grossi, C., Àgueda, A., Vogel, F. R., Vargas, A., Zimnoch, M., Wach, P., Martín, J. E., López-Coto, I., Bolívar, J. P., Morguá, J.-A., and Rodó, X.: Analysis of ground-based  $^{222}\text{Rn}$  measurements over Spain: filling the gap in southwestern Europe, *J. Geophys. Res.-Atmos.*, 121, 11021–11037, <https://doi.org/10.1002/2016JD025196>, 2016.
- Grossi, C., Vogel, F. R., Curcoll, R., Àgueda, A., Vargas, A., Rodó, X., and Morguá, J.-A.: Study of the daily and seasonal atmospheric  $\text{CH}_4$  mixing ratio variability in a rural Spanish region using  $^{222}\text{Rn}$  tracer, *Atmos. Chem. Phys.*, 18, 5847–5860, <https://doi.org/10.5194/acp-18-5847-2018>, 2018.
- Gutiérrez-Álvarez, I., Guerrero, J. L., Martín, J. E., Adame, J. A., Vargas, A., and Bolívar, J. P.: Radon behavior investigation based on cluster analysis and atmospheric modelling, *Atm. Environ.*, 201, 50–61, <https://doi.org/10.1016/j.atmosenv.2018.12.010>, 2019.
- Hernández-Ceballos, M. A., Vargas, A., Arnold, D., and Bolívar, J. P.: The role of mesoscale meteorology in modulating the  $^{222}\text{Rn}$  concentrations in Huelva (Spain) – impact of phosphogypsum piles, *J. Environ. Radioactiv.*, 145, 1–9, <https://doi.org/10.1016/j.jenvrad.2015.03.023>, 2015.
- Hirao, S., Yamazawa, H., and Moriizumi, J.: Inverse modelling of Asian  $^{222}\text{Rn}$  flux using surface air  $^{222}\text{Rn}$  concentration, *J. Environ. Radioactiv.*, 101, 974–984, <https://doi.org/10.1016/j.jenvrad.2010.07.004>, 2010.
- Hopke, P. K.: The initial behavior of  $^{218}\text{Po}$  in indoor air, *Environ. Int.*, 15, 299–308, 1989.
- Jacob, D. J. and Prather, M. J.: Radon-222 as a test of convective transport in a general circulation model. *Tellus B*, 42, 118–134, <https://doi.org/10.3402/tellusb.v42i1.15196>, 1990.
- Jacobi, W. and André, K.: The vertical distribution of radon 222, radon 220 and their decay products in the atmosphere, *J. Geophys. Res.*, 68, 3799–3814, 1963.
- IAEA (International Atomic Energy Agency): Sources and Measurements of Radon and Radon Progeny Applied to Climate and Air Quality Studies, in: Proceedings Series, Proceedings of a technical meeting, Vienna, Austria, organized by the International Atomic Energy Agency and co-sponsored by the World Meteorological Organization, IAEA, 59–62, 2012.
- Krystek, M. and Anton, M.: A weighted total least-squares algorithm for fitting a straight line, *Meas. Sci. Technol.*, 18, 3438, <https://doi.org/10.1088/0957-0233/18/11/025>, 2008.
- Levin, I., Glatzel-Mattheier, H., Marik, T., Cuntz, M., Schmidt, M., and Worthy, D. E. J.: Verification of German methane emission inventories and their recent changes based on atmospheric observations, *J. Geophys. Res.*, 104, 3447–3456, <https://doi.org/10.1029/1998JD100064>, 1999.
- Levin, I., Born, M., Cuntz, M., Langendörfer, U., Mantsch, S., Naegler, T., Schmidt, M., Varlagin, A., Verclas, S., and Wagenbach, D.: Observations of atmospheric variability and soil exhalation rate of Radon-222 at a Russian forest site: Technical approach and deployment for boundary layer studies, *Tellus B*, 54, 462–475, 2002.
- Levin, I., Hammer, S., Eichelmann, E., and Vogel, F. R.: Verification of greenhouse gas emission reductions: the prospect of atmospheric monitoring in polluted areas, *Philos. T. Roy. Soc. A*, 369, 1906–1924, 2011.
- Levin, I., Schmithüsen, D., and Vermeulen, A.: Assessment of  $^{222}\text{Rn}$  radon progeny loss in long tubing based on static filter measurements in the laboratory and in the field, *Atmos. Meas. Tech.*, 10, 1313–1321, <https://doi.org/10.5194/amt-10-1313-2017>, 2017.
- López-Coto, I., Mas, J. L., and Bolívar, J. P.: A 40-year retrospective European radon flux inventory including climatological variability, *Atmos. Environ.*, 73, 22–33, <https://doi.org/10.1016/j.atmosenv.2013.02.043>, 2013.
- Nazaroff, W. W. and Nero, A. V. (Eds.): Radon and its decay products in indoor air, *Physics Today* 42, 72, <https://doi.org/10.1063/1.2810982>, 1988.
- Karstens, U., Schwingshackl, C., Schmithüsen, D., and Levin, I.: A process-based  $^{222}\text{Rn}$  radon flux map for Europe and its comparison to long-term observations, *Atmos. Chem. Phys.*, 15, 12845–12865, <https://doi.org/10.5194/acp-15-12845-2015>, 2015.
- Paatero, J., Hatakka, J., and Viisanen, Y.: Concurrent measurements of airborne radon-222, lead-210 and beryllium-7 at the Pallas-Sodankylä GAW station, Northern Finland, Finnish Meteorological Institute, Helsinki, Report No. 1998:1, 1–30, 1998.
- Pereira, E. B. and da Silva, H. E.: Atmospheric radon measurements by electrostatic precipitation, *Nucl. Instrum. Meth. A*, 280, 503–505, 1989.
- Rosenfeld, M.: Modifikation des Heidelberger Radon-Monitors und erste Messungen, Diploma Thesis, University of Heidelberg, Heidelberg, Germany, 2010.
- Schery, S. D. and Huang, S.: An estimate of the global distribution of radon emissions from the ocean, *Geophys. Res. Lett.*, 31, L19104, <https://doi.org/10.1029/2004GL021051>, 2004.
- Schmithüsen, D., Chambers, S., Fischer, B., Gilge, S., Hatakka, J., Kazan, V., Neubert, R., Paatero, J., Ramonet, M., Schlosser, C., Schmid, S., Vermeulen, A., and Levin, I.: A European-wide  $^{222}\text{Rn}$  and  $^{222}\text{Rn}$  progeny comparison study, *Atmos. Meas. Tech.*, 10, 1299–1312, <https://doi.org/10.5194/amt-10-1299-2017>, 2017.
- Stockburger, H. und Sittkus, A.: Unmittelbare Messung der natürlichen und künstlichen Radioaktivität der atmosphärischen Luft, *Z. Naturforsch.*, 21, 1128–1132, 1966.
- Szegvary, T., Conen, F., and Ciais, P.: European  $^{222}\text{Rn}$  inventory for applied atmospheric studies, *Atmos. Environ.*, 43, 1536–1539, <https://doi.org/10.1016/j.atmosenv.2008.11.025>, 2009.
- Tositti, L., Pereira, E. B., Sandrini, S., Capra, D., Tubertini, O., and Bettoli, M. G.: Assessment of summer trends of tropospheric

- radon isotopes in a costal antarctic station (Terra Nova Bay), *Int. J. Environ. An. Ch.*, 82, 259–274, 2002.
- Vargas, A., Ortega, X., and Martín Matarranz, J. L.: Traceability of radon-222 activity concentration in the radon chamber at the technical university of Catalonia (Spain), *Nucl. Instrum. Meth. A*, 526, 501–509, <https://doi.org/10.1016/j.nima.2004.02.022>, 2004.
- Vargas, A., Arnold, D., Adame, J. A., Grossi, C., Hernández-Ceballos, M. A., and Bolívar, J. P.: Analysis of the vertical radon structure at the Spanish “El Arenosillo” tower station, *J. Environ. Radioactiv.*, 139, 1–17, <https://doi.org/10.1016/j.jenvrad.2014.09.018>, 2015.
- Vogel, F. R., Ishizawa, M., Chan, E., Chan, D., Hammer, S., Levin, I., and Worthy, D. E. J.: Regional non- $\text{CO}_2$  greenhouse gas fluxes inferred from atmospheric measurements in Ontario, Canada, *J. Integr. Environ. Sci.*, 9, 45–55, <https://doi.org/10.1080/1943815X.2012.691884>, 2012.
- Vogel, F. R., Tiruchittampalam, B., Theloke, J., Kretschmer, R., Gerbig, C., Hammer, S., and Levin, I.: Can we evaluate a fine-grained emission model using high-resolution atmospheric transport modelling and regional fossil fuel  $\text{CO}_2$  observations?, *Tellus B*, 65, 18681, <https://doi.org/10.3402/tellusb.v65i0.18681>, 2013.
- Wada, A., Matsueda, H., Murayama, S., Taguchi, S., Hirao, S., Yamazawa, H., Moriizumi, J., Tsuboi, K., Niwa, Y., and Sawa, Y.: Quantification of emission estimates of  $\text{CO}_2$ ,  $\text{CH}_4$  and CO for East Asia derived from atmospheric radon-222 measurements over the western North Pacific, *Tellus B*, 65, 18037, <https://doi.org/10.3402/tellusb.v65i0.18037>, 2013.
- Whittlestone, S. and Zahorowski, W.: Baseline radon detectors for shipboard use: Development and deployment in the First Aerosol Characterization Experiment (ACE 1), *J. Geophys. Res.*, 103, 16743–16751, <https://doi.org/10.1029/98JD00687>, 1998.
- Williams, A. G. and Chambers, S. D.: A history of radon measurements at Cape Grim, Baseline Atmospheric Program (Australia) History and Recollections, 40th Anniversary Special edn., 131–146, 2016.
- Williams, A. G., Zahorowski, W., Chambers, S., Griffiths, A., Hacker, J. M., Element, A., and Werczynski, S.: The vertical distribution of radon in clear and cloudy daytime terrestrial boundary layers, *J. Atmos. Sci.*, 68, 155–174, <https://doi.org/10.1175/2010JAS3576.1>, 2011.
- Williams, A. G., Chambers, S., and Griffiths, A.: Bulk mixing and decoupling of the nocturnal stable boundary layer characterized using a ubiquitous natural tracer, *Bound.-Lay. Meteorol.*, 149, 381–402, <https://doi.org/10.1007/s10546-013-9849-3>, 2013.
- Xia, Y., Sartorius, H., Schlosser, C., Stöhlker, U., Conen, F., and Zahorowski, W.: Comparison of one- and two-filter detectors for atmospheric  $^{222}\text{Rn}$  measurements under various meteorological conditions, *Atmos. Meas. Tech.*, 3, 723–731, <https://doi.org/10.5194/amt-3-723-2010>, 2010.
- Zahorowski, W., Chambers, S. D., and Henderson-Sellers, A.: Ground based radon-222 observations and their application to atmospheric studies, *J. Environ. Radioactiv.*, 76, 3–33, <https://doi.org/10.1016/j.jenvrad.2004.03.033>, 2004.